

APPLICATION OF COMPUTERS IN EXPERIMENTS

A Technique for the Mass Testing of Single-Sided Microstrip Detectors

P. F. Ermolov, A. G. Voronin, E. G. Zverev, D. E. Karmanov, E. N. Kuznetsov,
A. K. Leflat, M. M. Merkin, and E. K. Shabalina

Skobel'tsyn Institute of Nuclear Physics, Moscow State University, Vorob'evy gory, Moscow, 119899 Russia

Received February 8, 2001; in final form, June 8, 2001

Abstract—In 1986–2000, the Skobel'tsyn Institute of Nuclear Physics of Moscow State University took part in the development of a tracker for the D0 experiment (FERMILAB, USA) on the basis of microstrip silicon detectors. Using the mass testing of detectors for this experiment as an example, we describe a technique for testing single-sided microstrip detectors. The experimental results are presented for the detectors produced in Russia during 1998–2000.

1. SILICON SINGLE-SIDED MICROSTRIP DETECTORS FOR THE D0 EXPERIMENT

1.1. The Utilization of Microstrip Detectors in the D0 Experiment

The D0 experiment is a basic experiment with the Tevatron p^+p^- collider (FNAL, USA). The detecting system of the two fundamental Tevatron experiments (D0 and CDF) is currently refined, and this work involves the development of a tracker for the D0 experiment [1]. Its purpose is to reconstruct the positions of decays of short-lived p^+p^- -collision products with an accuracy within 10 μm . For this problem to be solved, single- and double-sided microstrip Si detectors are used in the D0 tracker as sensors. This detector type provides up to a 5- μm coordinate resolution with a ~ 10 -ns response time and good spectrometric properties (the signal-to-noise ratio for a signal from a minimum-ionizing particle is ~ 20).

The Si tracker for the D0 experiment consists of three main parts (Fig. 1): a central barrel, internal discs, and end discs. Each end disc incorporates 24 two-layer wedges; each wedge is composed of single-sided trapezoidal microstrip detectors glued together back-to-back (see [1]). The total number of detectors in the end discs is 384.

Skobel'tsyn Institute of Nuclear Physics (SINP) of Moscow State University participated in the development of the D0 tracker. The SINP specialists were engaged in testing the components of the end discs and assembling them. The total amount of detectors for these discs was 560 (including the necessary spare). The detectors were manufactured during 1998–2000 by NPO Elma (Zelenograd, Moscow) and tested at SINP.

1.2. Microstrip Detectors for the End Discs

The Si detectors of the end discs for the D0 experiment are single-sided microstrip detectors with p^+ -strips in the n -type material. A schematic diagram of a detector and a circuit diagram of its connection are shown in Fig. 2. The detectors are shaped as a trapezoid; their strips are parallel to the trapezoid's side [2]. Each wedge of a disc consists of two types of detectors: inner and outer. The basic detector dimensions are presented in Table 1; their electric parameters are the following. (1) The acceptable total leakage current I_{bias} of all strips at a 70-V voltage is 5 μA . (2) The polysilicon resistor of a strip has a resistance R_{Si} of $-1 \pm 0.2 \text{ M}\Omega$. (3) The full-depletion voltage of the detector U_{fd} is below 90 V. (4) The breakdown voltage of strip capacitors $U_{\text{AC max}}$ exceeds 60 V. (5) The maximum number of capacitors with a high leakage current ($I_{\text{cap}} > 5 \text{ nA}$ at 60 V) and strips with a high leakage current ($I_{\text{str}} > 10 \text{ nA}$ at an operating voltage) are four and eight, respectively. (6) The minimum interstrip resistance R_{intrst} is 1 $\text{G}\Omega$. (7) The linear capacitance of the strip's blocking capacitor $C_{\text{AC}} = 15 \pm 3 \text{ pF/cm}$, the linear capacitance of the strip to the back side of the detector C_{b} is $0.30 \pm 0.05 \text{ pF/cm}$, and the linear capacitance between two adjacent strips C_{s} is $1.5 \pm 0.2 \text{ pF/cm}$.

The operating voltage is applied to all detector strips over a bias line through polysilicon resistors $R_{\text{Si}} = 1.0 \pm 0.2 \text{ M}\Omega$. The signal is read out off every other strip by a charge-sensitive amplifier of a multichannel SVX2E integrated circuit. The SVX2E unpackaged integrated circuit amplifies, digitizes, and outputs the data from 128 detector strips [3]. The amplifier inputs are dc-voltage-isolated from the p^+ -strips by the blocking capacitors formed on the detector. These capacitors have double-layer isolators: the upper layer is silicon nitride, and the lower one is silicon oxide (Fig. 2 and Table 1).

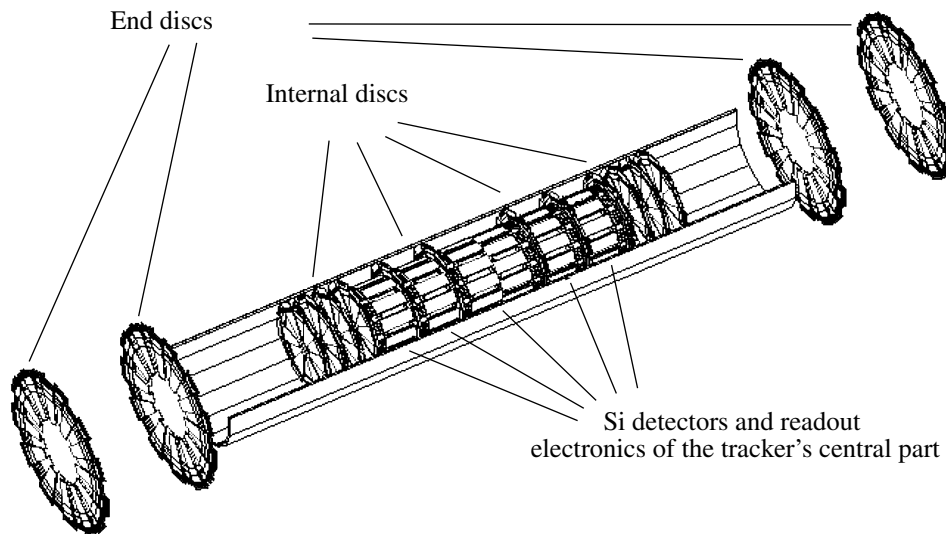


Fig. 1. Silicon tracker for the D0 experiment. General view and location of components.

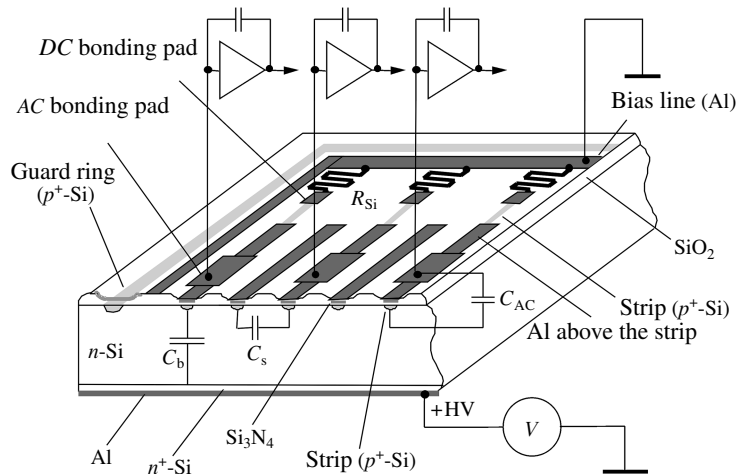


Fig. 2. Simplified construction of the microstrip end-disc detector and its connection to the readout electronics.

2. MASS TESTING OF MICROSTRIP DETECTORS

Estimating the quality of quantity-produced detectors is an important problem. Test results must not only present the characteristics of an instrument and its compliance to the specification but also provide a set of operating parameters for each detector and help monitor the adherence to the production process. With this aim in view, the following parameters are to be measured for each end-disc detector: (1) the full-depletion voltage U_{fd} , (2) the voltage dependence of the total detector current over a range of 0 V to $U_{fd} + 20$ V, (3) the leakage current of each blocking capacitor for voltages of 30 and 60 V, (4) the leakage current of each strip at 70 V, (5) the resistances of polysilicon detectors R_{Si} for a few strips, and (6) interstrip resistance R_{intrst} for a few strips. For individual detectors, it is necessary to measure (1) the capacitances of the strip's blocking

capacitor C_{AC} and of the strip to the back side of the detector C_b as well as the interstrip capacitance C_s , and (2) surface charge density in a thick oxide and at the Si-SiO₂ interface, produced, as a rule, while etching the passivation.

The capacitance parameters C_{AC} , C_b , and C_s depend on the detector configuration and, partly, on the surface charge density in the strip region. This fact allows us to carry out mass testing of the detectors by measuring these parameters only for individual strips on a few wafers from each lot. If the parameters of a sample do not comply with the specifications, additional measurements are required to check the adherence to the detector-manufacturing technology and the quality of silicon, e.g., measurements of (1) the contact resistance of aluminum to the polysilicon resistor and to the p^+ -implantation region of the strip, (2) contact resis-

Table 1. Basic detector dimensions

Parameter	External detector	Internal detector
Major base of trapezoid, mm	64.780	47.980
Trapezoid height, mm	64.500	76.870
Number of strips	1562	1126
Length of Al metallization on the full-length strips, mm	65.150	77.250
Angle of strips with the normal to the trapezoid base, deg	7.5	
Strip spacing, μm	40	
Width of the strip p^+ -region, μm	8 ± 0.5	
Width of the aluminum above the doped region, μm	14 ± 0.5	
Insulator thickness between the p^+ -region and Al, μm :		
top layer, SiO_2	0.12 ± 0.02	
bottom layer, Si_3N_4	0.12 ± 0.02	
Detector thickness, μm	300 ± 15	

tance of the aluminum to silicon on the back side of the detector, (3) dielectric breakdown voltage in the blocking capacitor, (4) resistance of the strip aluminum metallization $R_{\text{Al str}}$, and (5) resistance of the strip p^+ -implantation R_p .

Measuring the parameters of the detector itself is not enough for these values to be determined; some of them can be correctly measured only with special test structures that are not parts of the detector. They are manufactured together with the detector on the same Si wafer in the same production cycle.

When the scope of measurements is large (>100 detectors), it is particularly important to rapidly process the experimental data and visualize the results. The use of software that combines the functions of a measuring program with database functions seems to be the best solution of this problem. A simple method for creating such a hybrid is provided by the MS EXCEL table processor. The software used by SINP for testing the D0 detectors is based on the EXCEL table. It comprises the following components: (1) measured parameters of each detector in an easily readable form; (2) several VBA macros that are responsible for the data processing for each type of measurements, e.g., the computation of U_{fd} , R_{Si} , R_{intrst} , and surface charge density; (3) two universal measuring VBA macros, one of which is used in measuring the currents and the other determines the capacitance characteristics of the detector; and (4) several service tables containing standard parameters for each measurement type.

The structure of the program and interaction of its parts are presented in Fig. 3.

2.1. General Requirements to the Measuring Equipment

Some specific conditions are to be satisfied in the investigations. In particular, the detector must be

proofed against light in each measurement. In addition, the p - n -junction leakage (e.g., strip current) should be measured at a fixed temperature that is the closest possible to the operating temperature of the detector.

Probe stations form the basis of the setups for determining the detector parameters. Some parameters can be measured using stations with manual probe positioning; the other tasks (e.g., the search for broken strips and capacitors on the strips) require the use of automated probe stations providing a displacement accuracy within $1 \mu\text{m}$ per 10 cm and a minimum step of $\leq 10 \mu\text{m}$. The maximum displacement of the probes in the automatic mode is 10 cm or more.

The pressure of the probe tip on the detector is an important parameter of the probes for hand-operated and automated probe stations. In these experiments, the probes with a needle-tip diameter of 8 – $10 \mu\text{m}$ are pressed to the detector surface with a force of $\sim 0.04 \text{ N}$. The force value selected by experiment provides a reliable contact with the aluminum on the detector surface without any damage to the underlying layers.

The minimum kit for testing single-sided microstrip detectors contains the following instruments: (1) a controlled voltage source with a range of 0 – 500 V and 1-V step; (2) a controlled bipolar low-voltage source with a range of -10 to $+10 \text{ V}$ and 0.1-V step; (3) a controlled relay switch for 4 – 8 channels with a maximum switched voltage of above 200 V ; (4) a digital current meter with a resolution of 0.01 nA or better; (5) a digital capacitance meter with a range of 0.1 – 10^4 pF , testing-pulse height $\leq 100 \text{ mV}$, and a set of operating frequencies from 0.1 to 1000 kHz .

The GPIB interface is the most commonly used standard for controlling this type of meters. As a rule, techniques for measuring the detector parameters demand from the instruments and software reliable operation for a few hours, but a fast response is not necessary.

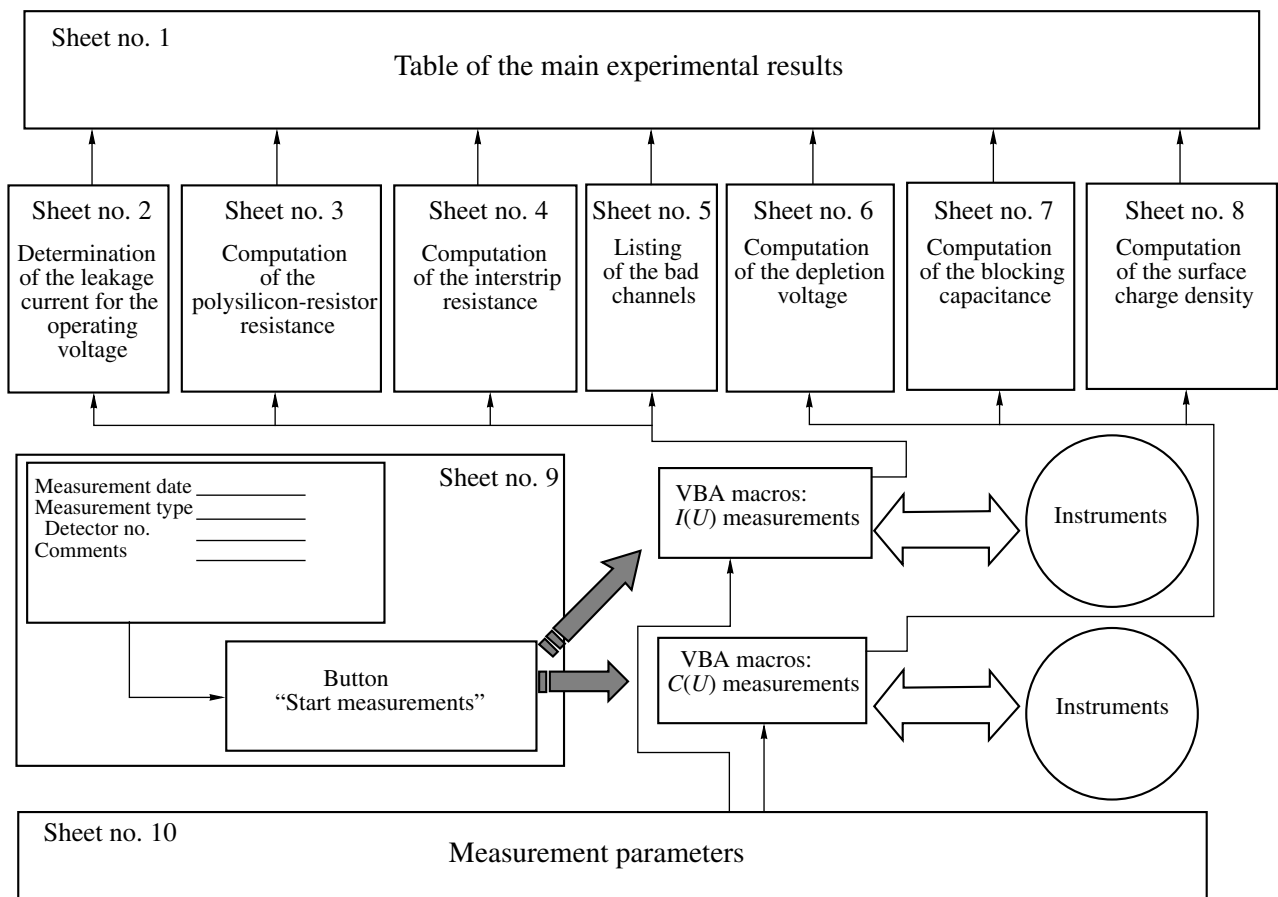


Fig. 3. Block diagram of the measurement program for testing the end-disc detectors.

3. BASIC CIRCUITS FOR MEASURING THE DETECTOR PARAMETERS

Below, we present circuits for measuring the detector parameters and the methods for their computation. We also describe some test structures produced to determine the parameters that cannot be correctly measured with the detector itself.

3.1. Total-Current Measurements

A circuit for measuring the total current of a single-sided microstrip detector is presented in Fig. 4. A characteristic dependence $I(U)$ for the end-disc detectors is shown in Fig. 5. The detectors operate with the p^+ -type guard rings being isolated. In this case, the total current in the detector is equal to the current in the detector's bias line.

The measurement of the total current in the detectors whose guard rings are supposed to be kept at a fixed potential requires that some probes and a switch be included in the measuring circuit. In this case, the total detector current is equal to either the sum of successively measured currents from the bias line and from each of the connected guard rings or the current simultaneously measured from the probes, which are con-

nected in parallel and attached to the bus and all of the rings.

The first type of measurements is more informative, because it allows one to reveal which part of the detector (strips or the interface region) makes the major contribution to the leakage current. However, it should be taken into account that, sequentially connecting the ammeter to each probe through the switch without the simultaneous connection of the remaining probes to the given potential (in this case, to the ground, see Fig. 4), we obtain an incorrect, overestimated current value. In such a circuit, for each structure under investigation, a portion of the current is diverted from the adjacent disconnected structures in the ammeter.

3.2. Measuring the Leakage Currents of Strips

The leakage currents of the strips are measured in much the same way as the total current is but with the use of the automated probe station. A relay multiplexer sequentially connects probes nos. 1 and 2 to a picoammeter (Fig. 4). A characteristic profile of the strip currents is shown in Fig. 6a for an internal detector of the end disc. Starting from the 580th strip, the strip currents decrease, because the strips become shorter.

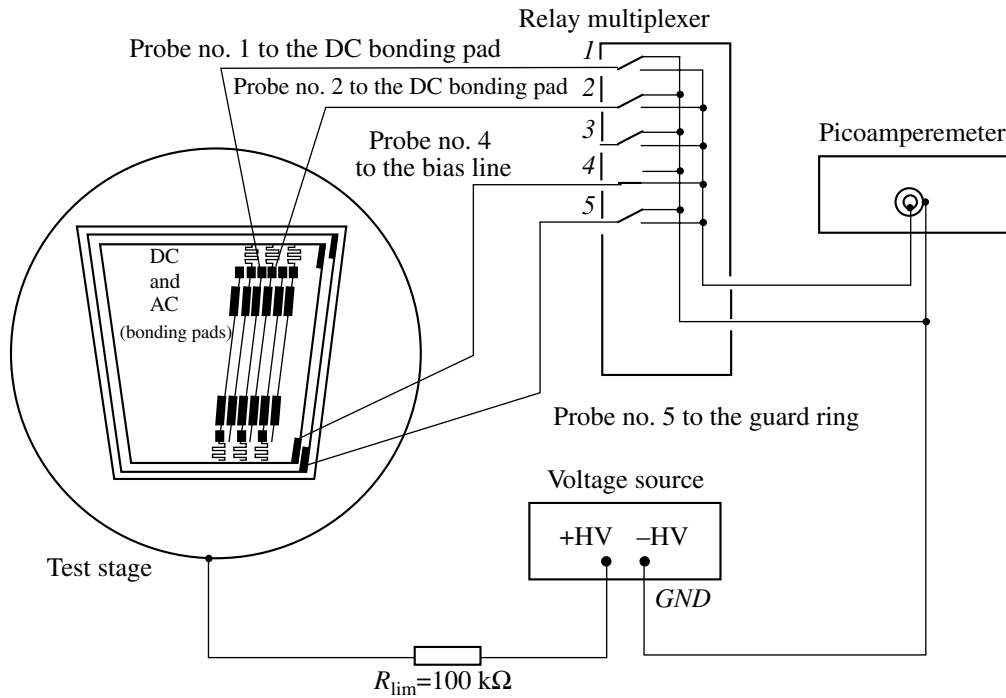


Fig. 4. Connection of the devices to the detector for measuring the strip leakage currents.

While measuring the strip currents, one of the probes (no. 4 in Fig. 4) must permanently connect the bias line to the ground of the measuring circuit. It is necessary to monitor the quality of this contact, because, when the contact resistance R_{prob} at this point increases, a portion of the total detector current is added to the measured strip currents,

$$I_{\text{meas}} = I_{\text{str}} + I_{\text{com}}(R_{\text{com}} + R_{\text{prob}})/R_{\text{Si}}, \quad (1)$$

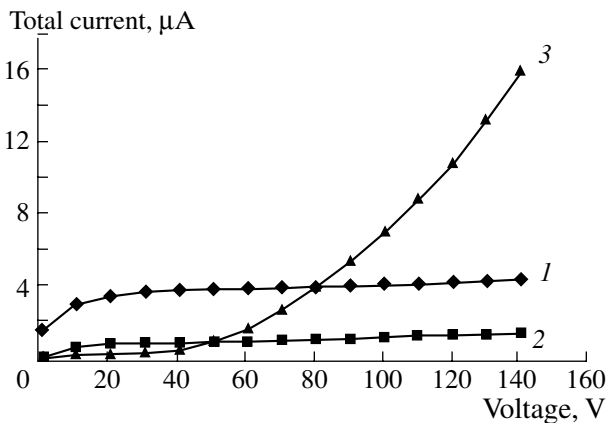


Fig. 5. Voltage dependence of the leakage current for three detectors: (1) Si with a reduced carrier lifetime; (2) Si with a normal lifetime; and (3) increase in the generation current because of the Si defects at the back of the wafer.

where $R_{\text{Si}} = 1 \text{ M}\Omega$ is the resistance of the polysilicon resistor; R_{com} the fraction of the aluminum resistance of the bias line, corresponding to the distance along the bus from the strip at hand to the point where the fourth probe is hooked up.

Another salient feature of the strip-current measurements is the fact that, in the detectors under investigation, every other strip at different bases of the trapezoid is connected to the bias line. At the same time, the configurations of the probe station and detector permit measurements along one base only. As a result, in the measurements of the strip leaks on the longer base of the trapezoid, the current of the strip connected to the bus at the shorter side (even strips) is divided between the bus and the picoamperemeter:

$$I_{\text{meas}} = I_{\text{str}}R_{\text{Si}}/(R_{\text{Si}} + R_p), \quad (2)$$

where R_p is the resistance of the p^+ -implantation strip region from the point where the probe is hooked up to the polysilicon resistor (Fig. 4).

The R_p resistance nonlinearly varies with the voltage applied. For these detectors, the strip-implantation resistance per unit length is $r_p = 60 \pm 20 \text{ k}\Omega/\text{cm}$ for voltages of $\sim 1.0 \text{ V}$. We see that the current measured in an even strip decreases by 0.1–0.15 nA (20–30%) at these resistance values. This effect is insignificant for odd strips connected to the bus at the longer side (at a place where the current is measured), since only the input resistance of the picoamperemeter (which is 0.1–10 kΩ depending on the measurement range) acts as R_p .

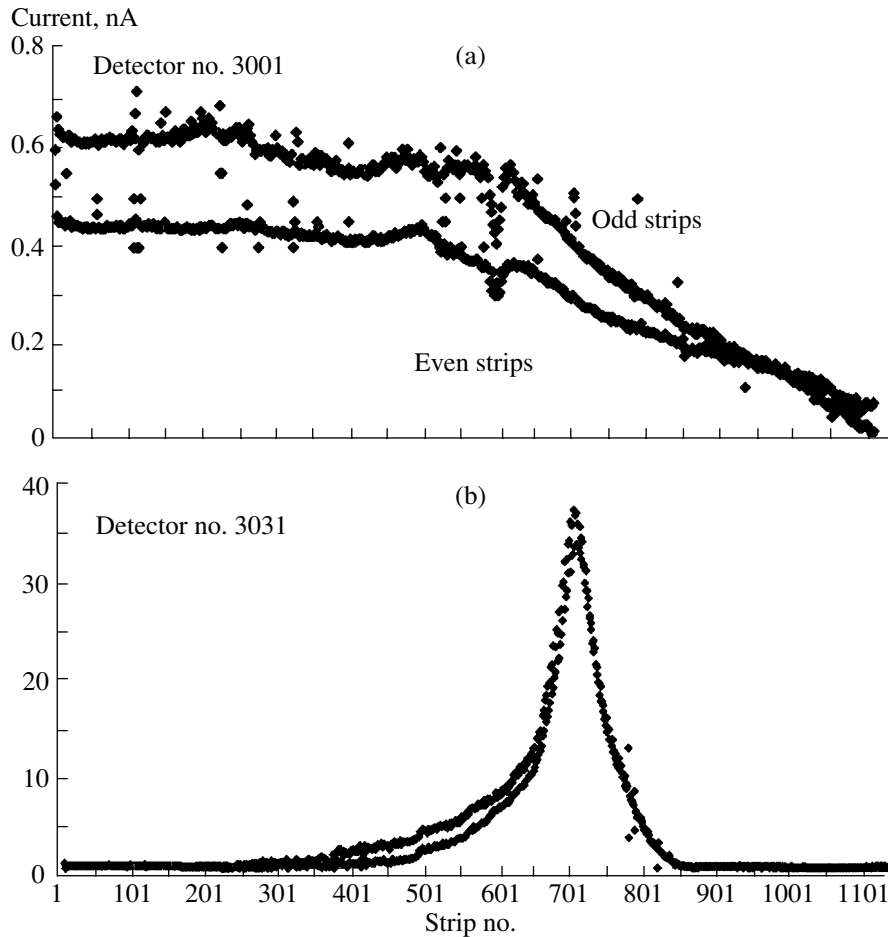


Fig. 6. Leakage currents of the strip (a) at normal and (b) low interstrip resistance. The operating voltage is 70 V.

Another effect arising when the strip currents change is attributed to the influence of interstrip resistance. With $R_{\text{intrst}} < 10 \text{ M}\Omega$, the leakage currents from the strips that are adjacent to the strip under investigation are distributed between it and the bias line. This results in the overestimation of the measured strip current, which increases with a decrease in R_{intrst} .

The low-resistance region conventionally includes a few tens to a few hundred strips. Incidentally, the total leakage current of the entire detector I_{com} becomes several times less than the sum of the leakage currents from all the strips. Such behavior indicates that the interstrip resistance is low and measurements of the strip currents are incorrect. A characteristic profile of the strip currents at a low interstrip resistance is shown in Fig. 6b for an internal end-disc detector.

Hence, the accuracy of direct strip-current measurements at low contact resistances at the probe sites and a high interstrip resistance is within 20–30% for even strips and 5% for odd ones. At the same time, these effects give rise to systematic errors and can be compensated according to Eqs. (1) and (2) if the R_{Si} , R_{com} , and R_p values are known. Moreover, these measure-

ments, even without any compensation, provide much knowledge on the quality of the p – n junctions of the strips.

3.3. Measuring the Leakage Currents of Blocking Capacitors

When mounting the readout electronics on the microstrip detector, defective strips, i.e., strips with large leakage currents of p – n junctions and with punched blocking capacitors, are supposed not to be connected, because the electronics may be damaged by the high voltage from the strip through a broken capacitor.

The setup for checking the capacitor quality includes the automated probe station with same devices as for strip leakage current measurements (Fig. 4), but probes nos. 1 and 2 should be installed on AC pads, and probes nos. 4 and 5 are disconnected. The testing voltage is connected to the p – n junction of the strip in the forward direction such that the voltage drop at the junction is only 1 V and virtually the entire voltage is applied to the insulator of the blocking capacitor. The

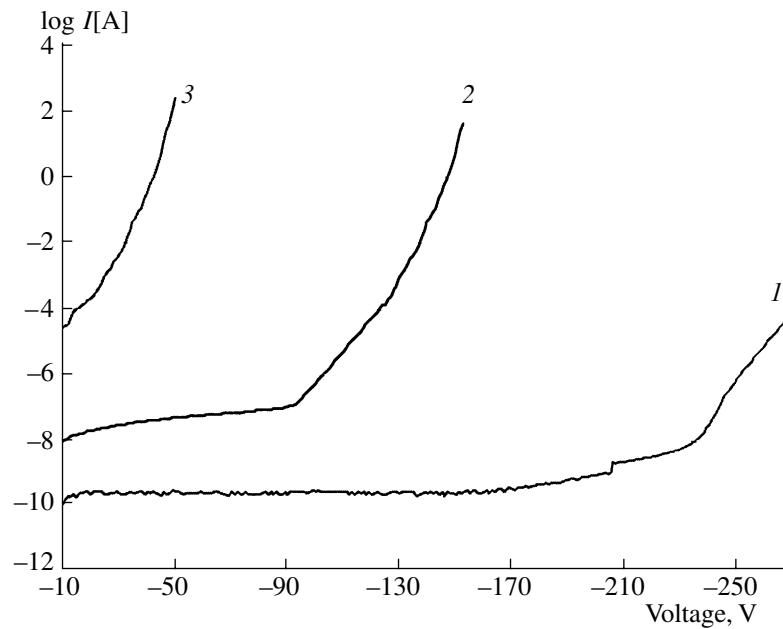


Fig. 7. Leakage currents of the blocking capacitors as functions of voltage for three strips on different detectors [(1, 3) with the detector no. 3040 and (2) with the detector no. 1153]: (1) normal quality of both insulator layers; (2) reduced thickness and a high imperfection of the thin oxide; and (3) a “hole” in both insulator layers.

current-limiting resistance $R_{lim} = 1 \text{ M}\Omega$ makes it impossible to damage the p - n junction if the capacitor is broken down.

Apart from searching for the punched capacitors, the setup helps investigate the dielectric-breakdown behavior in the strip capacitor. Consider three possible voltage dependences of the capacitor-leakage current (Fig. 7). All of the curves represent the experimental data.

The function 3 corresponds to a hole in both dielectric layers, which may be brought about by a photomask defect or by a dust microparticle on the strip surface during photolithography over the silicon nitride. A direct contact is thus produced between the capacitor plates (Al and p^+) over the defect area.

Curve 2 corresponds to the reduced thickness and high imperfection of the thin oxide. In this case, the capacitor leakage significantly exceeds the normal value, because silicon nitride at room temperature yields a resistance of $\sim 10 \text{ G}\Omega$ and a leakage of 5 nA over a $\sim 0.5\text{-mm}^2$ strip area at a 50-V voltage and a $\sim 0.1\text{-}\mu\text{m}$ strip thickness [4]. The breakdown voltage in this case is lower than the required value of 100 V, because the testing voltage is actually applied to one dielectric layer.

Curve 1 is plotted for the normal quality of both dielectric layers. The breakdown voltage is calculated as follows:

$$U_{AC \max} = E_{\max \text{ SiO}_2} d_{\text{SiO}_2} + E_{\max \text{ Si}_3\text{N}_4} d_{\text{Si}_3\text{N}_4}, \quad (3)$$

where $E_{\max \text{ SiO}_2} = 9 \cdot 10^6 \text{ V/cm}$ is the breakdown strength of SiO_2 [4], $d_{\text{SiO}_2} = 0.12 \text{ }\mu\text{m}$ is the silicon oxide thick-

ness in the double-layer capacitor dielectric, $E_{\max \text{ Si}_3\text{N}_4} = 7.2 \times 10^6 \text{ V/cm}$ is the breakdown strength of Si_3N_4 at room temperature [4], and $d_{\text{Si}_3\text{N}_4} = 0.12 \text{ }\mu\text{m}$ is the silicon nitride thickness. Hence, $U_{AC \max} = 195 \text{ V}$, which agrees with the measured breakdown voltage (curve 1 in Fig. 7).

Note that the leakage current of the capacitor with a normal dielectric quality is very small at voltages $< 150 \text{ V}$, and the current measured at a 60-V voltage is the charging current of the capacitor upon applying the voltage step to it. This current conventionally falls down to the noise level within 5–20 s (at a current-limiting resistance of $1 \text{ M}\Omega$).

The other defect of the blocking capacitor is due to breaks of the strip metallization. They are responsible for a loss of the signal from particles that were incident onto the strip farther away from the break point (counting off from the strip end to which the amplifier is connected). A break of the aluminum film can result, mainly, from the overetching if the sequence of operations is violated at the stage of photolithography on aluminum or from the incidence of a dust microparticle on the strip at the same stage. In the first case, many (> 10) strips are conventionally broken, and a few separate strips may be broken in the second case.

A decrease in the current recharging the capacitor in a capacitor-leakage measurement is an indirect indication that the strip is broken. The direct test is to measure the metallization resistance between two probes installed at the opposite strip ends. The setup for checking the capacitors, supplemented with the second probe, is used in these measurements as well. The test-

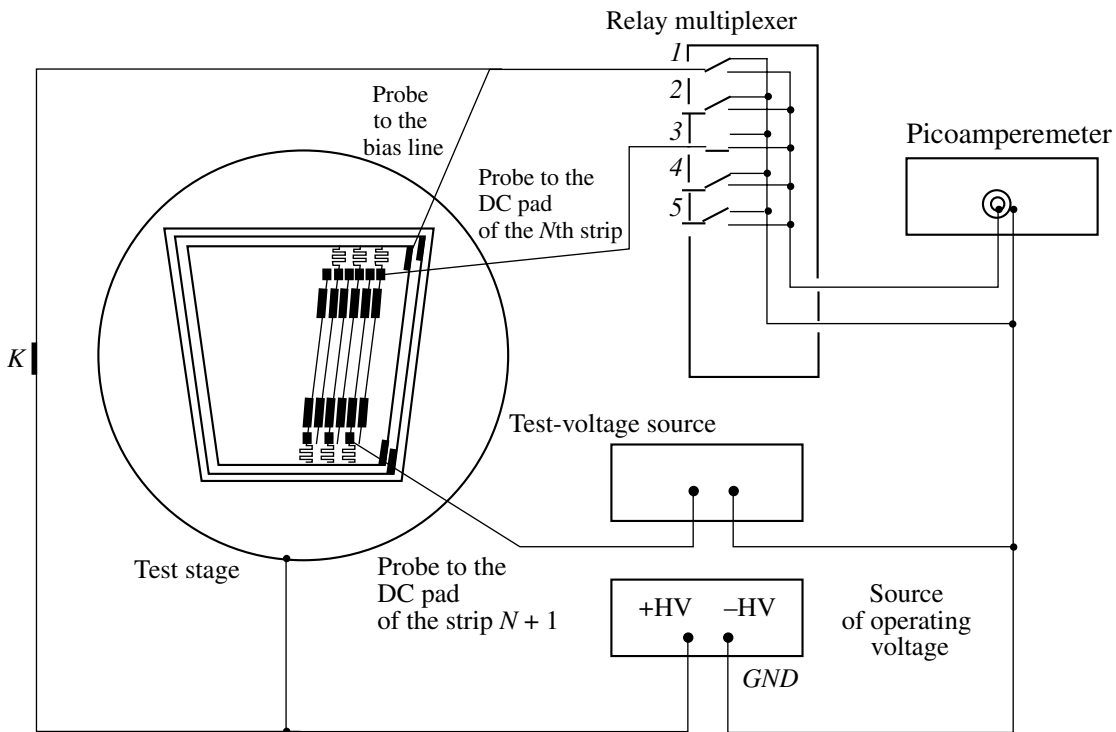


Fig. 8. Connection of the detector and devices for measuring the resistances of polysilicon resistors (switch *K* is closed and the test-voltage source is disconnected) and the interstrip resistance (switch *K* is open, the test-voltage source is connected and switched on).

ing voltage is applied between the probes. The measured resistance of the aluminum metallization per unit length is $r_{Al\ str} = 50 \pm 15 \Omega/cm$. The spread in resistance is attributed to different etching of aluminum in different lots; for the same lot, this spread is within 10%.

3.4. Resistances of Polysilicon Resistors

The circuit diagram presented in Fig. 8 is used to measure the resistance of polysilicon resistors R_{Si} . The testing voltage is applied to the strip's *p-n* junction in the opposite direction; the polysilicon resistor of the

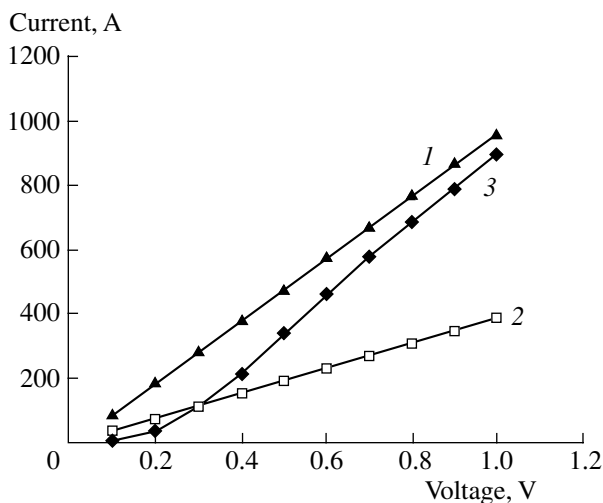


Fig. 9. Dependence of the current through the polysilicon resistor on the test voltage: (1) normal quality of polysilicon resistor; (2) increased polysilicon resistance; and (3) nonlinear contact resistance of the polysilicon resistor to aluminum.

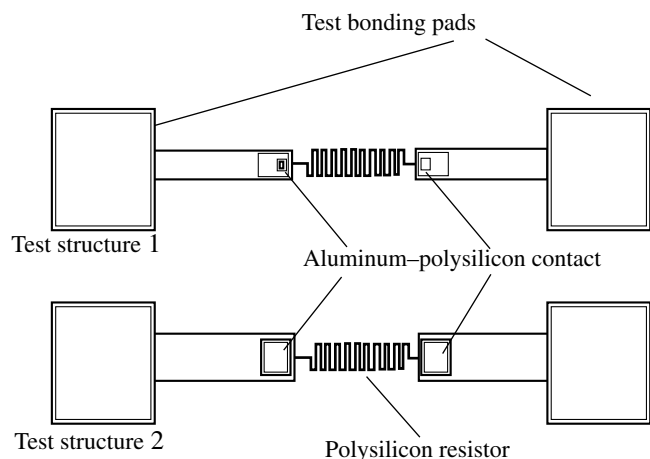


Fig. 10. Test structures for examining the polysilicon resistors with normal (test structure 1) and increased contact area of polysilicon to aluminum (test structure 2).

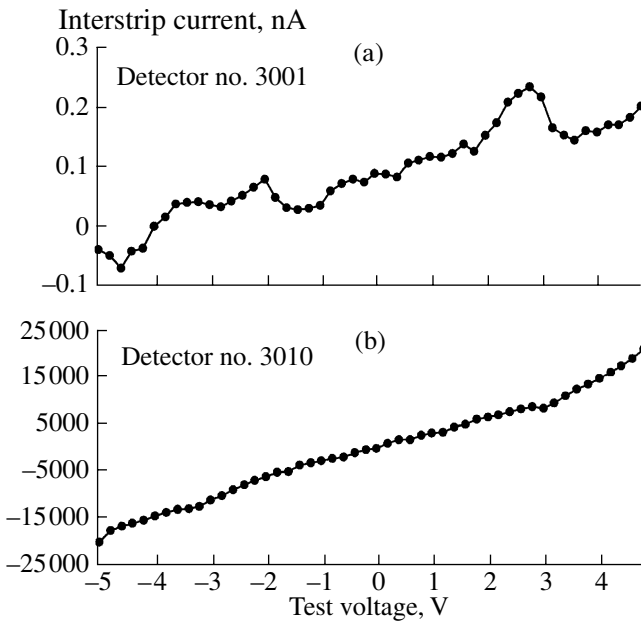


Fig. 11. Dependence of the current between two neighbor strips on the voltage applied to them (a) for normal and (b) reduced interstrip capacitance. The normal resistance is $\sim 40 \text{ G}\Omega$ and the reduced one is $\sim 250 \text{ k}\Omega$.

strip is connected in parallel to the junction. Since the resistance of the closed junction in the normal strip far exceeds the value $R_{Si} = 1 \text{ M}\Omega$, this junction does not affect the measurement accuracy.

Two types of the polysilicon-resistor defects are found: a discrepancy between the resistance and the specifications (Fig. 9, curve 2) and nonlinear resistance at low testing voltages (Fig. 9, curve 3). The first defect is due to both the nonobservance of the resistor dimensions in the etching of the polysilicon and errors in the impurity dosage in the doping of the polysilicon, which cause its resistivity to depart. The other defect results from the occurrence of nonlinear resistance at a point of the aluminum-to-polysilicon contact.

The test structures (Fig. 10) help precisely determine the point of increased contact resistance. If the condition $R_{Si(s)} \gg R_{Si(nom)}$ is satisfied for the strip resistances measured at low voltages and $R_{Si(t1)} = R_{Si(t2)} = R_{Si(nom)}$ for the test structures, we infer that the p^+ -strip-to-aluminum contact at the bonding pad is bad. On the other hand, if $R_{Si(s)} \gg R_{Si(nom)}$ for the strips, but, for the test structures, $R_{Si(t2)} = R_{Si(nom)}$ and $R_{Si(t1)} \gg R_{Si(nom)}$, a bad contact is considered to exist between the resistor and aluminum at the bonding pad.

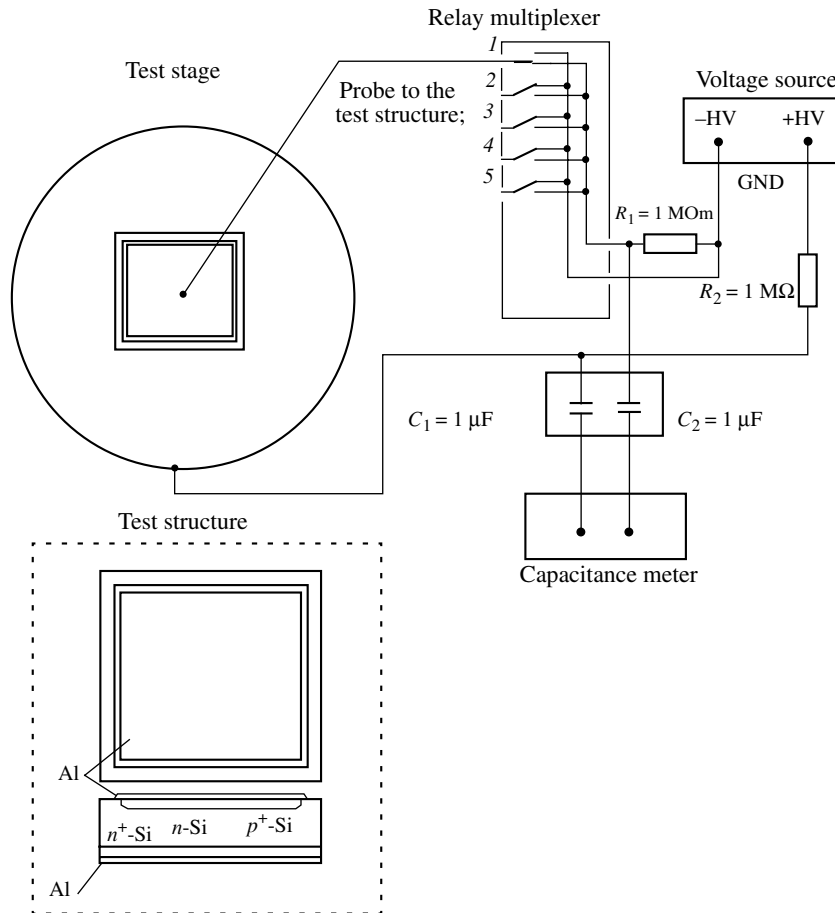


Fig. 12. Connection of the instruments to the test structure for measuring the full-depletion voltage by the $C(U)$ dependence.

3.5. Interstrip-Resistance Measurements

A block diagram of the interstrip-resistance measurements is shown in Fig. 8. The experimental dependences of the interstrip current on the testing voltage are given in Figs. 11a and 11b, respectively, for normal and low interstrip resistances. The detector should be at an operating voltage of 70 V during the measurements. The testing voltage applied between the strips varied from -1.0 to +1.0 V with a 0.02-V step.

3.6. Determination of the Full-Depletion Voltage

The full-depletion voltage is measured by the $1/C^2$ technique with the test structure that is a $p-n$ junction of a 5.5×5.5 -mm area (Fig. 12). The test structure and the detector are located on the same wafer and produced in the common technological cycle.

The essence of the $1/C^2$ technique is to measure the $p-n$ -junction capacitance of the test structure versus the cutoff voltage applied to the junction. Using the square test structure of a large size compared to the wafer thickness makes it possible to represent the processes in the $p-n$ -junction with a one-dimensional approximation.

The experimental dependence $1/C^2(U)$ for a test structure is shown in Fig. 13. The full-depletion voltage U_{fd} is defined as a voltage at which the dependence attains a plateau. Here, $U_{fd} = 50$ V. The rising linear section of the $1/C^2(U)$ dependence provides information on the silicon resistivity ρ , which is assumed to be the same over the wafer depth [5]:

$$\rho = \epsilon_0 \epsilon_{Si} S^2 / 2 \mu_{Si} U C^2, \quad (4)$$

where $\epsilon_{Si} = 12$ is the silicon permittivity; U is the cutoff voltage applied to the junction; $\mu_{Si} = 1500 \text{ cm}^2/(\text{V s})$ is the electron mobility in Si; S is the $p-n$ -junction area; C is the test-structure capacitance at a voltage U . For the sample from Fig. 13, we obtain $\rho = 5.8 \text{ k}\Omega \text{ cm}$.

The capacitance at a given voltage presents information on the depletion depth at this voltage:

$$d(U) = \epsilon_0 \epsilon_{Si} S / C(U). \quad (5)$$

The full-depletion depth for Fig. 13 at a 50-V voltage is

$$d_{fd} = 289 \text{ }\mu\text{m} \quad (C_{fd} = 12.8 \text{ pF at } U_{fd} = 50 \text{ V}).$$

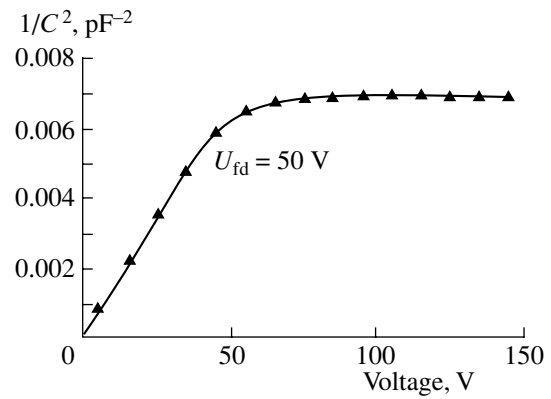


Fig. 13. Voltage dependence of $1/C^2$.

3.7. Interstrip Capacitance

The interstrip capacitance is an important parameter of the microstrip detector, which affects the coordinate resolution and the particle-detection efficiency [6]. Through their complexity, the interstrip-capacitance measurements are not mandatory for each detector. The measurements were carried out at FNAL (USA) with the ALESSI-6500 manual probe station and a few detectors that were cut out but not connected to the electronic circuits. The probes were set upon the strip metallization on the AC bonding pads (Fig. 2), i.e., on the bonding pads of the blocking capacitor. The measurements were performed at a 100-Hz frequency using an HP-4284 multifrequency LCR-meter. An operating voltage of 70 V was applied to the detectors.

The main difficulty in determining the interstrip capacitance is to eliminate the effect of additional capacitances, i.e., capacitances of the neighbor strips and capacitance of the analyzed strip to the opposite side of the detector. For the interstrip capacitance to be discerned among them, several measurements were made with differing numbers and configurations of the connected strips. The circuit diagrams for their connection are shown in Fig. 14.

Table 2 presents the experimental results for probes connected in different circuits and the appropriate expressions for the measured capacitances, where C_m is the measured capacitance; C_b is the capacitance of a

Table 2. Measured capacitances of the external and internal (in brackets) detectors

Circuit no.	Equivalent circuit	Spurious capacitance, pF	Measured C_m value without the spurious capacitance, pF
1	$C_m = C_b + 2C_a$	0.2 (0.2)	7.9 ± 0.1 (8.4 ± 0.1)
2	$C_m = 2C_b + 2C_a$	0.7 (0.8)	9.7 ± 0.1 (10.0 ± 0.1)
3	$C_m = 3C_b + 2C_a$	1.6 (1.7)	10.9 ± 0.1 (11.7 ± 0.1)
4	$C_m = C_b + 2C_s$	0.2 (0.2)	20.1 ± 0.1 (21.5 ± 0.1)
5	$C_m = C_b + C_a + C_s$	0.2 (0.2)	14.7 ± 0.1 (15.4 ± 0.1)

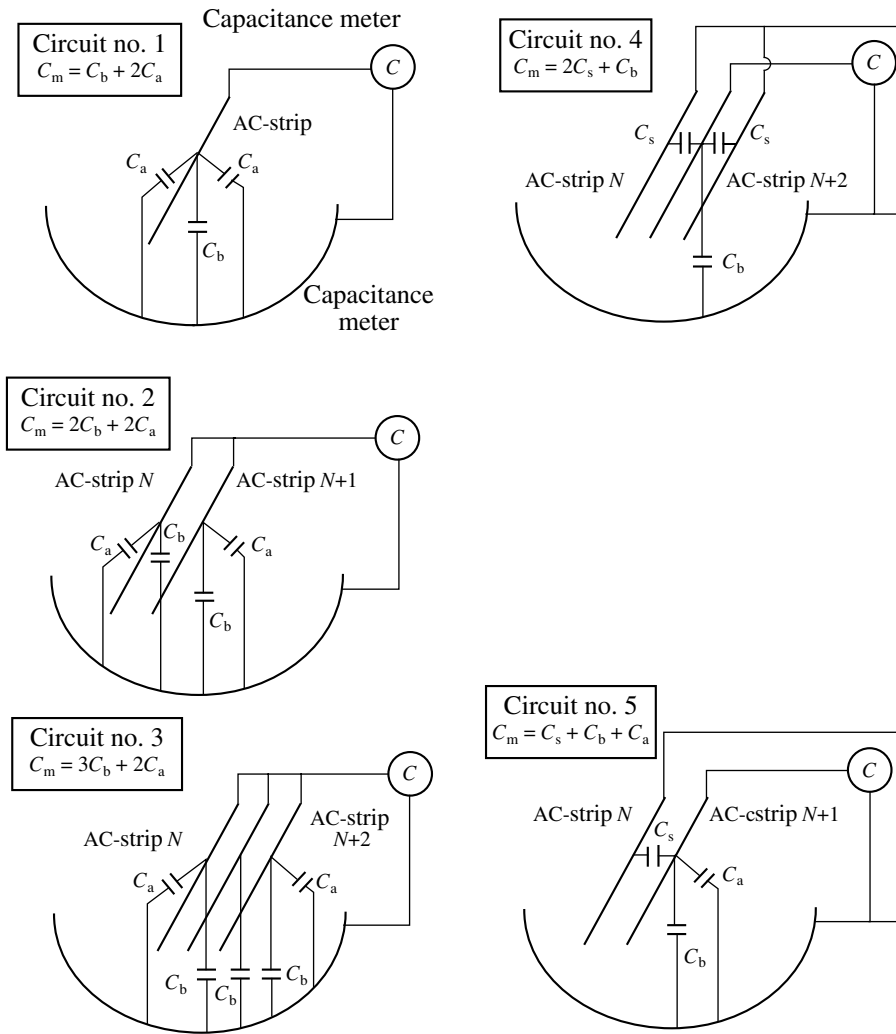


Fig. 14. Circuits of probe connection for measuring the interstrip capacitance.

single strip to the back side of the detector; C_a is the aggregate capacitance of one strip to the back side of the detector due to all adjacent strips on the right and the left of it; and C_s is the interstrip capacitance. Any group of these three expressions can be considered as a system of three equations with three unknown quantities: C_b , C_a , and C_s . Solving different combinations of equations and normalizing the results by the strip length, we obtain the following values of linear capacitance:

$$c_b = 0.23 \pm 0.06 \text{ pF/cm},$$

$$c_s = 1.50 \pm 0.07 \text{ pF/cm},$$

and $c_a = 0.50 \pm 0.07 \text{ pF/cm}$.

3.8. Blocking Capacitance

Designing of a microstrip detector imposes contradictory requirements for the blocking-capacitor components. On the one hand, the dielectric in a capacitor

has to be thick, so that it can bear a voltage above 60 V. On the other hand, the capacitance C_{AC} should be as large as possible in order to avoid losses of the charge collected from the ionizing particle in the $C_b - C_{AC}$ capacitive voltage divider. In this case, increasing the plate area is undesirable, since it causes the capacitance of the strip to the back side to increase by itself.

A combination of Si_3N_4 ($\epsilon_{\text{Si}_3\text{N}_4} = 6.5$) and SiO_2 ($\epsilon_{\text{SiO}_2} \approx 3.6$), see Table 1, is used in the blocking capacitors of the disc detectors. It provides a sufficiently large capacitance and a high breakdown voltage. In this case, the blocking capacitance of the strip is described by the expression for the capacitance of a plane capacitor with double-layer dielectric (the factor $\lambda = 1.23$ takes into account the actual capacitor geometry),

$$C_{AC} = \lambda(\epsilon_0 \epsilon_{\text{SiO}_2} L_{\text{Al}} D_p / d_{\text{SiO}_2}) \Pi(\epsilon_0 \epsilon_{\text{Si}_3\text{N}_4} L_{\text{Al}} D_p / d_{\text{Si}_3\text{N}_4}), \quad (6)$$

where L_{Al} is the length of the aluminum film on the strip, D_p is the width of the p^+ -implantation in the strip, d_{SiO_2} is the SiO_2 thickness in the double-layer dielectric, $d_{\text{Si}_3\text{N}_4}$ is the Si_3N_4 thickness in the double-layer dielectric,

and Π denotes the series connection of capacitors. The estimated blocking capacitance per unit strip length in the disc detectors is

$$c_{AC} = 17 \text{ pF/cm.}$$

Two probes were used to measure the blocking capacitance. One of them was set up upon the strip metallization and the AC bonding pad; the other was attached to the DC bonding pad connected to the strip p^+ -implantation region (Fig. 2). The detector was not in the depleted state during the measurements; i.e., the operating voltage was not applied.

The distributed plate resistance is the major difficulty in the capacitance measurements. Using the strip-metallization resistance per unit length $r_{Al\text{str}}$ from Section 3.3 and the resistance of the p^+ -implantation region per unit length r_p from Section 3.2, it is possible to estimate the resistances of the blocking-capacitor plates. For a strip length of ~ 6 cm, the impedance of the top aluminum plate is $\sim 300 \Omega$ and that of the bottom plate (p^+ -implantation) is $\sim 300 \text{ k}\Omega$.

The E7-14 LCR-meter with an operating frequency of 1 kHz was used in the measurements. In order to take into account the plate resistances, the measurements were carried out in the C_s - R mode, in which the object under investigation was considered as a capacitor and resistor connected in series. Under these conditions, the measured blocking capacitance per unit strip length was

$$c_{AC} = 13.0 \pm 2.0 \text{ pF/cm}$$

for detectors from different lots. This value was less than the calculated capacitance. The difference was due to the inaccurate account of the ohmic loss, because the actual strip circuit is not simply a series connection of a capacitor and resistor but a distributed RC-circuit.

3.9. Measuring the Surface Charge Density in Oxide

Three-layer metal-insulator-semiconductor (MIS) structures are often used to determine the parameters of oxides and other dielectric films on the Si surface. A fundamental characteristic of a MIS structure that reflects the insulator parameters and, eventually, the quality of the production process is the voltage dependence of the structure capacitance.

The MIS-structure capacitance is a series connection of the dielectric-layer capacitor C_d and capacitor of the near-surface depletion region of the semiconductor C_{depl} . In the MIS structure with n -Si, the positive voltage applied to the aluminum above the insulator attracts electrons of the n -Si to the Si surface, thus producing a region rich in carriers. Incidentally, the MIS-structure capacitance is virtually independent of the voltage; it is $C_{max} = C_d$.

On the contrary, the negative voltage U applied to the metal above the insulator repels electrons of n -Si from the surface, producing the depleted region with a capacitance C_{depl} ; in this case, the total capacitance decreases. The positive surface charge with a density σ

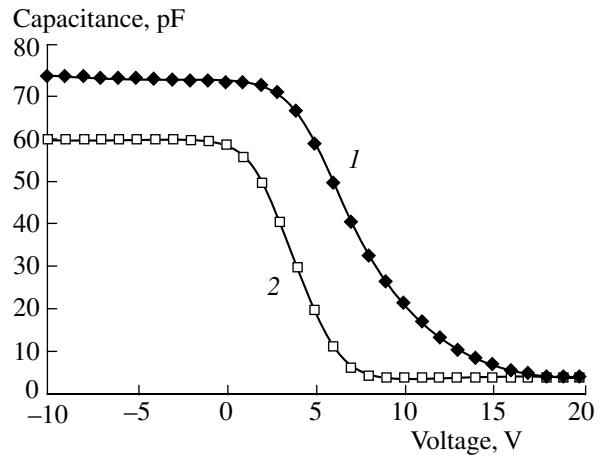


Fig. 15. Capacitance of the test MIS structures as a function of voltage: (1) Al-SiO₂- n -Si structure and (2) Al-Si₃N₄-SiO₂- n -Si structure.

at the insulator-semiconductor interface attracts electrons of n -Si to the surface. As a result, the near-surface Si layer becomes depleted at external negative voltages higher in modulus.

The point of inflection in the graph of MIS-structure capacitance against voltage (Fig. 15) corresponds to the so-called flat-band voltage U_{fb} , where the field of the surface charge is balanced by the external electric field,

$$U_{fb} = -\sigma e d_d / (\epsilon_0 \epsilon_d). \quad (7)$$

In the case of double-layer dielectric, Eq. (7) takes the form

$$U_{fb} = -\sigma e (d_{d2} / \epsilon_0 \epsilon_{d1} + d_{d1} / \epsilon_0 \epsilon_{d2}). \quad (7a)$$

These conditions correspond to the case where the field and the potential at the n -Si boundary are zero and the entire surface charge is concentrated at the oxide-silicon interface.

The surface-charge density at the silicon-insulator interface was measured with special MIS structures of 1×1 -mm area (Table 3). An E7-14 LCR-meter with a built-in bipolar voltage source was used to measure the capacitance. The operating frequency was 1 kHz. For the influence of the Si series resistance to be neutralized, the measurements were carried out in the C_s - R mode.

The capacitances of the test MIS structures versus the bias voltage are shown in Fig. 15 for detector number 1443. The C_{max} and U_{fb} values, measured with the test structures of this detector, are presented in Table 3. Using the C_{max} values and the test-structure areas, the dielectric-layer thicknesses d_{d1} and d_{d2} are calculated. Then, from the measured value of U_{fb} , the surface charge density σ is found by Eqs. (7) and (7a).

The experimental results obtained with the test structures of 20 detectors are the following:

- (1) The charge under the thick oxide layer (without silicon nitride)

Table 3. Parameters and characteristics of the test MIS structures

Layers	Experimental data		Calculation		
	C_{\max} , pF	U_{fb} , V	Layer thickness, μm		Surface charge density, $10^{11} e/\text{cm}^2$
			SiO_2 (d_{d1})	Si_3N_4 (d_{d2})	
Al-SiO ₂ - <i>n</i> -Si	74.7	7.5	0.43	No layer	3.5
Al-Si ₃ N ₄ -SiO ₂ - <i>n</i> -Si	59.6	3.5	0.43	0.19	1.3

$$\begin{aligned}\sigma_1 &= (2.9 \pm 1.3) \times 10^{11} e/\text{cm}^2 \\ &= (4.6 \pm 2.0) \times 10^{-4} \text{ C/m}^2;\end{aligned}$$

(2) The charge under the thick oxide layer with the nitride above

$$\begin{aligned}\sigma_2 &= (1.3 \pm 0.4) \times 10^{11} e/\text{cm}^2 \\ &= (2.0 \pm 0.6) \times 10^{-4} \text{ C/m}^2.\end{aligned}$$

We see that adding the silicon nitride layer reduces the measured value of the total surface charge. This may be brought about by the motion of the surface charge from the SiO₂ film towards the SiO₂-Si₃N₄ interface. Note that the quantity σ_1 is the most important parameter for estimating the detector quality, since the structure of the regions near the strip edges is metal-thick oxide-*n*-Si. A large surface charge can cause a premature breakdown of the strip *p*-*n* interfaces, a breakdown of the blocking-capacitor dielectric [7], and an increase in the surface currents.

CONCLUSION

The detectors for the tracker of the D0 experiment have been produced and tested by November 2000. From September 1998 to October 2000, more than 1700 detectors for the end discs were manufactured by NPO Elma and tested by SINP; 576 of them were accepted for assembling the discs. At present, the discs have been assembled and installed in the beam. The tracker of the D0 experiment was started in April 2001. The testing of its components on the beam and preparation for the data acquisition are currently under way.

ACKNOWLEDGMENTS

We thank N.V. Baranova, G.A. Bogdanova, V.N. Volkov, M.A. Pereletova, and N.S. Petrusевич for useful advices and help; A.I. Sidorov, N.N. Egorov, S.A. Golubkov, and other employees of NPO Elma for participating in the production of the end-disc detectors.

We are also grateful to our US colleagues—Dr. R. Lipton and Prof. J. Elisson—for inviting SINP to take part in developing the tracker for the D0 experiment and for the steady support.

This work was supported by the CRDF Foundation, grant no. RE 2-142, 1996–1998.

REFERENCES

1. D0 Upgrade Collaboration, *D0 Note no. 2169*, Batavia: FNAL, 1994.
2. Ermolov, P., Merkin, M., Shabalina, L., *et al.*, *Preprint of Institute of Nuclear Physics, Moscow State Univ.*, Moscow, 1997, no. 97-22/473.
3. Yarema, R., *FERMILAB-TM-1892*, Batavia: FNAL, prepared 1994, revised 1996.
4. Sze, S.M., *Physics of Semiconductor Devices*, New York: Wiley, 1981, vol. 1. Translated under the title *Fizika poluprovodnikovykh priborov*, Moscow: Mir, 1981, vol. 1, p. 428.
5. Tugov, N.M., Glebov, B.A., and Charykov, N.A., *Poluprovodnikovye pribory* (Semiconductor Devices), Moscow: Energoatomizdat, 1990, p. 60.
6. Zverev, E.G., Karmanov, D.E., Leflat, A.K., *et al.*, *Preprint of Institute of Nuclear Physics, Moscow State Univ.*, Moscow, 1998, no. 98-37/538.
7. Angelescu, T., Mihul, A., Militaru, O., *et al.*, *Preprint of Univ. of Bucharest*, Bucharest, 1998, no. EPPG/PHYS 38.